JOURNAL OF VIROLOGY, July 2009, p. 6631–6640 Vol. 83, No. 13
0022-538X/09/$08.00+0 doi:10.1128/JVI.00367-09

Molecular Determinants for Subcellular Localization of the Severe Acute Respiratory Syndrome Coronavirus Open Reading Frame 3b Protein▽

Eric C. Freundt,[1,2] Li Yu,[1] Elizabeth Park,[1] Michael J. Lenardo,[1] and Xiao-Ning Xu[2]*

Laboratory of Immunology, Institute of Allergy and Infectious Diseases, National Institutes of Health, Bethesda, Maryland 20892,[1] and Medical Research Council Human Immunology Unit, Weatherall Institute of Molecular Medicine, John Radcliffe Hospital, University of Oxford, Oxford OX3 9DS, United Kingdom[2]

Received 18 February 2009/Accepted 16 April 2009

Viruses such as hepatitis C and the severe acute respiratory syndrome coronavirus (SARS-CoV) encode proteins that are distributed between mitochondria and the nucleus, but little is known about the factors that control partitioning between these sites. SARS-CoV encodes a unique accessory gene called open reading frame (ORF) 3b that, like other unique accessory genes in SARS-CoV, likely contributes to viral pathogenicity. The ORF 3b protein is 154 amino acids and is predicted to express from the second ORF in subgenomic RNA3. In this report, we have characterized the molecular components that regulate intracellular localization of the ORF 3b protein. We demonstrate unique shuttling behavior of ORF 3b, whereby the protein initially accumulates in the nucleus and subsequently translocates to mitochondria. Following nuclear localization, ORF 3b traffics to the outer membrane of mitochondria via a predicted amphipathic α-helix. Additionally, ORF 3b contains a consensus nuclear export sequence, and we demonstrate that nuclear export and thus mitochondrial translocation are dependent on a leptomycin B-sensitive nuclear export mechanism. We further show that ORF 3b inhibits induction of type I interferon induced by retinoic acid-induced gene 1 and the mitochondrial antiviral signaling protein. Our observations provide insights into the cellular localization of ORF 3b that may enhance our understanding of the mechanisms by which ORF 3b contributes to SARS-CoV pathogenesis. The findings reported here reveal that for multilocalized proteins, consideration of the spatiotemporal distribution may be crucial for understanding viral protein behavior and function.

The severe acute respiratory syndrome coronavirus (SARS-CoV) emerged in 2003 and caused a multinational epidemic. SARS-CoV is characterized by a 100-nm enveloped virion containing the spike glycoprotein, the membrane glycoprotein, small envelope protein, and the 3a glycoprotein (19, 22). Additional proteins associated with the viral particle include nucleocapsid phosphoprotein (N) and open reading frame (ORF) 6 protein (21). The 29,751-nucleotide genome of SARS-CoV is composed of single-stranded, positive-sense RNA and is predicted to contain 15 ORFs. The SARS-CoV genome encodes eight smaller ORFs located in the 3′ end of the genome that are predicted to express eight proteins that are novel even among other known human CoVs. Five of these eight group-specific ORFs, including ORFs 3a, 3b, 6, 7a, and 7b, were deleted from recombinant SARS-CoV and found to be dispensable for viral replication both in tissue culture and in mice (40). It is therefore likely that these five accessory proteins promote specialized viral replication or modulate host immune responses (31). Detailed characterization of these novel proteins should contribute to a better understanding of both SARS pathogenesis and the challenges viruses face in host tissues.

One of the unique proteins is encoded by ORF 3b, the second ORF in subgenomic RNA3 (32). Also known as X2 or ORF 4, the ORF 3b protein is predicted to be 154 amino acids long, and current evidence suggests that ORF 3b may be expressed during infection (4, 16). The precise determinants of intracellular localization of ORF 3b are not yet understood. Certain studies have reported both mitochondrial and nucleolar localization of ORF 3b, whereas others have detected only nuclear localization (25, 41, 43). Importantly, ORF 3b has been shown to antagonize cellular production of type I interferon (IFN) (25). Additional studies suggest that ORF 3b might be involved in initiating host cell apoptosis although these have been contested (24, 42).

In the present study, we report unique localization behavior of ORF 3b, whereby the protein initially accumulates in the nucleus and subsequently translocates to mitochondria. The molecular determinants of subcellular localization include a CRM1-dependent nuclear export sequence and a predicted amphipathic α-helix necessary for binding to the outer membrane of mitochondria. Within this predicted helix, two lysine residues are important to mediate mitochondrial localization. Finally, we confirm previous findings demonstrating an inhibitory role for ORF 3b in type I IFN signaling and suggest that the inhibitory effect of ORF 3b occurs at or downstream of the mitochondrial antiviral signaling (MAVS) protein. These findings may contribute to understanding the mechanism by which ORF 3b contributes to SARS-CoV pathogenesis.

* Corresponding author. Mailing address: Medical Research Council Human Immunology Unit, Weatherall Institute of Molecular Medicine, John Radcliffe Hospital, University of Oxford, Oxford OX3 9DS, United Kingdom. Phone: 44 1865 222401. Fax: 44 1865 222628. E-mail: xiaoning.xu@imm.ox.ac.uk.

▽ Published ahead of print on 29 April 2009.

TABLE 1. Oligonucleotides used for cloning and site-directed mutagenesis

Primer name[a]	Primer sequence (5′-3′)
3b FOR	CCGGAATTCATGATGCCAACTACTTTGTTTGCTGG
3b REV	TCCCCCCGGGCACGTACCTGTTTCTTCCGAA
1 FOR	GGGAATTCCACCATGATGCCAACTACTTTGTTTGCTGG
20 FOR	GGGAATTCCACCATGACAGTGTCACAGATACAATTGT
70 Rev	ACACCGGTGCAAACTTCGGTGAAATAGCCATGTAC
90 REV	ACACCGGTGCAGAATGTAGCATTTTCAATACCAGTG
110 REV	ACACCGGTGCAGCCGTCGATTGTGTGTATTTGCA
130 REV	ACACCGGTGCTAGTAGTCGTCGTCGGCTCATCA
L74A FOR	GAAGTTTACTACCAGCGCGAGTCTACACAAATTA
L74A REV	TAATTTGTGTAGACTCGCGCTGGTAGTAAACTTC
K78A FOR	CCAGCTTGAGTCTACACGCATTACTACAGACACTGG
K78A REV	CCAGTGTCTGTAGTAATGCGTGTAGACTCAAGCTGG
L79A FOR	CTTGAGTCTACACAAAGCACTACAGACACTGGTATTG
L79A REV	CAATACCAGTGTCTGTAGTGCTTTGTGTAGACTCAAG
L83A FOR	CAAATTACTACAGACAGCGGTATTGAAAATGCTACATTC
L83A REV	GAATGTAGCATTTTCAATACCGCTGTCTGTAGTAATTTG
V84A FOR	CAAATTACTACAGACACTGGCATTGAAAATGCTACATTC
V84A REV	GAATGTAGCATTTTCAATGCCAGTGTCTGTAGTAATTTG
K86A FOR	ACAGACACTGGTATTGGCAATGCTACATTCTTCATC
K86A REV	GATGAAGAATGTAGCATTGCCAATACCAGTGTCTGT
L88A FOR	CACTGGTATTGAAAATGGCACATTCTTCATCTTTAACAAGC
L88A REV	GCTTGTTAAAGATGAAGAATGTGCCATTTTCAATACCAGTG
L93A FOR	ATGCTACATTCTTCATCTGCAACAAGCTTGTTAAAGAC
L93A REV	GTCTTTAACAAGCTTGTTGCAGATGAAGAATGTAGCAT

[a] FOR, forward; REV, reverse.

MATERIALS AND METHODS

Plasmids. Reverse transcription followed by PCR was carried out using the gene-specific primers 3b FOR and 3b REV (Table 1). Resulting PCR products were subjected to restriction digestion and cloned into the EcoRI-XmaI sites of the p3xFlag-EGFP vector, which expresses ORFs fused to enhanced green fluorescent protein (EGFP) under the control of the cytomegalovirus promoter. The absence of unintended mutations in the resulting construct was confirmed by sequencing. For cloning of truncated forms of ORF 3b, gene-specific primers were designed to amplify DNA coding for amino acids 20 to 154, 1 to 70, 1 to 90, 1 to 110, and 1 to 130 (Table 1). PCR products were digested and cloned into the EcoRI and AgeI sites of the vector pEGFP-N1 (BD Biosciences, Clontech, Palo Alto, CA). Rev-GFP was kindly provided by Diane Bolton (National Institute of Allergy and Infectious Diseases [NIAID], National Institutes of Health). A constitutively active form of the retinoic acid-induced gene 1 (RIG-I-N) expression construct and IFN regulatory factor 3 (IRF-3) luciferase reporter plasmids were gifts from Takashi Fujita (Kyoto University), and the pRLTK reporter construct was purchased from Promega. The expression construct for MAVS was from Zhijian Chen (University of Texas Southwestern Medical Center).

Site-directed mutagenesis. Mutagenesis of the wild-type protein was carried out by PCR, followed by DpnI digestion using primers described in Table 1.

Cell culture and transfection. Vero and HEK293T cells were obtained from the American Type Culture Collection (Rockville, MD). Cells were maintained in Dulbecco's modified Eagle's medium with 4.5 g/liter glucose, supplemented with 2 mM L-glutamine, 1% penicillin-streptomycin solution, and 10% fetal bovine serum. HEK293T cells were transfected by the calcium phosphate precipitation method using 1 μg of DNA. Vero cells (1×10^6) were transfected with 0.5 μg of DNA by Amaxa nucleofection, using solution V and Amaxa program T-16 (Gaithersburg, MD). Where indicated in the figures, cells were cultured in the presence of 5 ng/ml leptomycin B (LMB) (Sigma).

Microscopy. Transfected cells were subcultured in a four-chamber borosilicate chambered coverglass system (Nunc) and imaged live under a confocal fluorescence microscope using a 63× oil immersion objective (Leica SP5; Leica Microsystems, Wetzlar, Germany). During imaging, cells were maintained at 37°C and 5% CO_2, and laser power was kept at minimal intensity to limit cytotoxicity. To assess intracellular localization, cells were stained with 20 nM MitoTracker Red CMXRos or 1 μg/ml Hoechst 33342 (Invitrogen-Molecular Probes, Carlsbad, CA).

FRAP. Fluorescence recovery after photobleaching (FRAP) analysis was done on Vero cells transfected as above with EGFP fused to the C terminus of ORF 3b (ORF 3b-EGFP). Images were acquired from cells cultured in phenol red-free Dulbecco's modified Eagle's medium with 5% fetal bovine serum. The microscope stage was heated to 37°C and a 63× objective was used. Defined regions of the cells were photobleached with the 488-nm line of a 400-mW Ar/Kr laser using 100% laser output for 15 iterations. Recovery of fluorescence was monitored by scanning the regions of interest once per second for at least 15 s after photobleaching. Mean fluorescence intensity of the regions of interest were calculated and plotted versus time with LAS AF software and the FRAP wizard program (Leica).

Subcellular fractionation and proteinase K digestion. Mitochondria were isolated by Percoll gradient centrifugation, using a mitochondrial isolation kit (Sigma) according to manufacturer's instructions. Briefly, 20 million transfected HEK293T cells were harvested in mitochondrial lysis buffer (10 mM HEPES, pH 7.5, 200 mM mannitol, 70 mM sucrose, 1 mM EGTA), supplemented with complete protease inhibitor cocktail (Roche), and homogenized for 60 to 70 strokes with a Dounce homogenizer. Samples were then transferred to Eppendorf tubes and centrifuged at 600 × *g* for 5 min at 4°C to eliminate nuclei and unbroken cells. The cytosolic fraction was collected from the supernatant after another centrifugation at 10,000 × *g* for 10 min at 4°C. The pellet was resuspended in Percoll solution (30% Percoll, 225 mM mannitol, 25 mM HEPES, 0.5 mM EGTA, and 0.1% bovine serum albumin) and ultracentrifuged at 40,000 × *g* for 1 h at 4°C. The mitochondria (the most prominent layer) were removed by syringe and washed with phosphate-buffered saline. The mitochondrial fraction was then incubated with 0 or 10 μg/ml proteinase K (Sigma) for 30 min at 25°C, at which time the digestion was stopped by the addition of phenylmethylsulfonyl fluoride (Sigma) to a final concentration of 2 mM. Mitochondrial samples were lysed with 2% sodium dodecyl sulfate lysis buffer before analysis by immunoblotting.

Immunoblot analysis. Lysates were boiled in reducing sample buffer and separated by sodium dodecyl sulfate-polyacrylamide gel electrophoresis using Novex 4 to 12% Bis-Tris gels. (Invitrogen) and immunoblotted using anti-Flag M2 (Sigma), anti-Tom20 (Santa Cruz Biotechnologies, Santa Cruz, CA), or anti-oxidative phosphorylation complex I (OxPhos-I) (Invitrogen-Molecular Probes) as described previously (44).

Dual luciferase reporter assays. HEK293T cells were cotransfected with 0.25 μg of the reporter plasmid containing the NF-κB or IRF-3 promoter linked to firefly luciferase and 40 ng of the *Renilla* luciferase reporter plasmid (pRLTK), which is constitutively expressed. Cells were also cotransfected with 1 μg of a plasmid expressing ORF 3b or empty vector and 0.5 μg of empty vector, RIG-I-N, or MAVS constructs for stimulation. Transfected cells were assayed 16 h posttransfection (hpt). Where indicated, cells were treated with 10 ng/ml human tumor necrosis factor alpha (TNF-α; R&D Systems) for 6 h prior to analysis. Cells were lysed in 500 μl of passive lysis buffer for at least 30 min and mixed, and

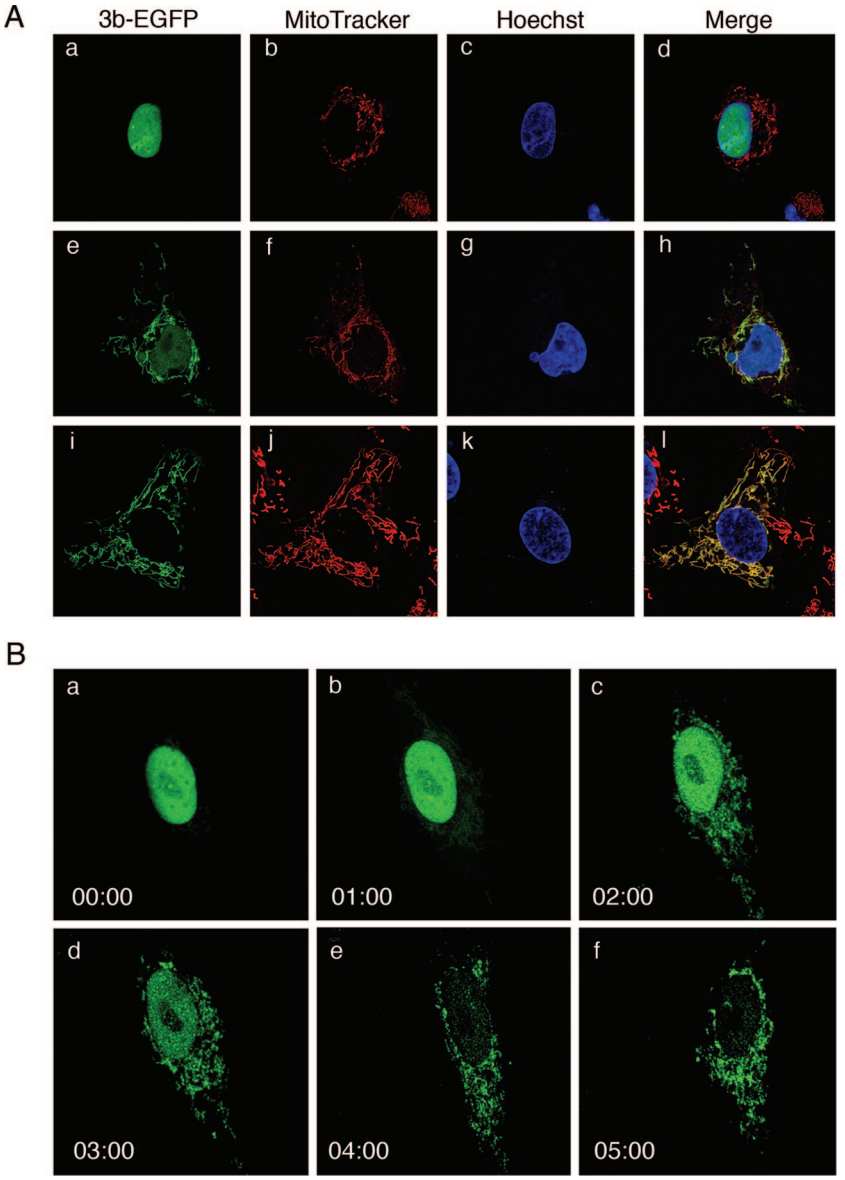

FIG. 1. Confocal analysis of the intracellular localization of the SARS-CoV ORF 3b. (A) Vero cells were transfected with ORF 3b-EGFP, counterstained with MitoTracker (red) or Hoechst (blue) to identify mitochondria and nuclei, respectively, and observed by confocal microscopy. Cells were observed that displayed exclusively nuclear (a to d), nuclear and mitochondrial ORF 3b (e to h), and exclusively mitochondrial (i to l) localization of ORF 3b. (B) Time-lapse microscopy of a single live Vero cell expressing ORF 3b-EGFP starting at 24 hpt. Images were captured every hour for 5 h, as indicated at the bottom left of each image.

20 μl of the lysate was added per well to a 96-well plate. Samples were mixed with 100 μl of luciferase substrate, and the firefly luciferase activity was quantitated. Samples were then mixed with 100 μl of Stop and Glow buffer (Promega), and *Renilla* luciferase activity was quantitated. All samples were analyzed using a Fluostar Optima luminometer according to the Promega protocol. After it was verified that all readings were in the linear range of the assay, firefly luciferase activity was divided by the *Renilla* luciferase activity to yield relative luciferase units (RLU).

RESULTS

Subcellular localization of ORF 3b. Previous reports have described both nuclear and mitochondrial locations for ORF 3b, but the findings have been discrepant (25, 41, 43). We examined the live intracellular localization of ORF 3b by expressing ORF 3b-EGFP. Vero cells expressing the ORF 3b-EGFP plasmid were analyzed by confocal microscopy after costaining for the nucleus and mitochondria with Hoechst and MitoTracker Red dyes, respectively, was performed. In support of previous reports, we found cells in which ORF 3b was localized to both the nucleus and to mitochondria (Fig. 1A). We did not, however, as has been described, observe ORF 3b localized in the nucleolus (43). Rather, for those cells in which nuclear localization was observed, ORF 3b was evenly distributed throughout the nucleus (Fig. 1A). At 16 hpt, we observed cells that displayed both nuclear and mitochondrial localization of ORF 3b. Additionally, we discerned cells with exclusively nuclear or exclusively mitochondrial ORF 3b protein.

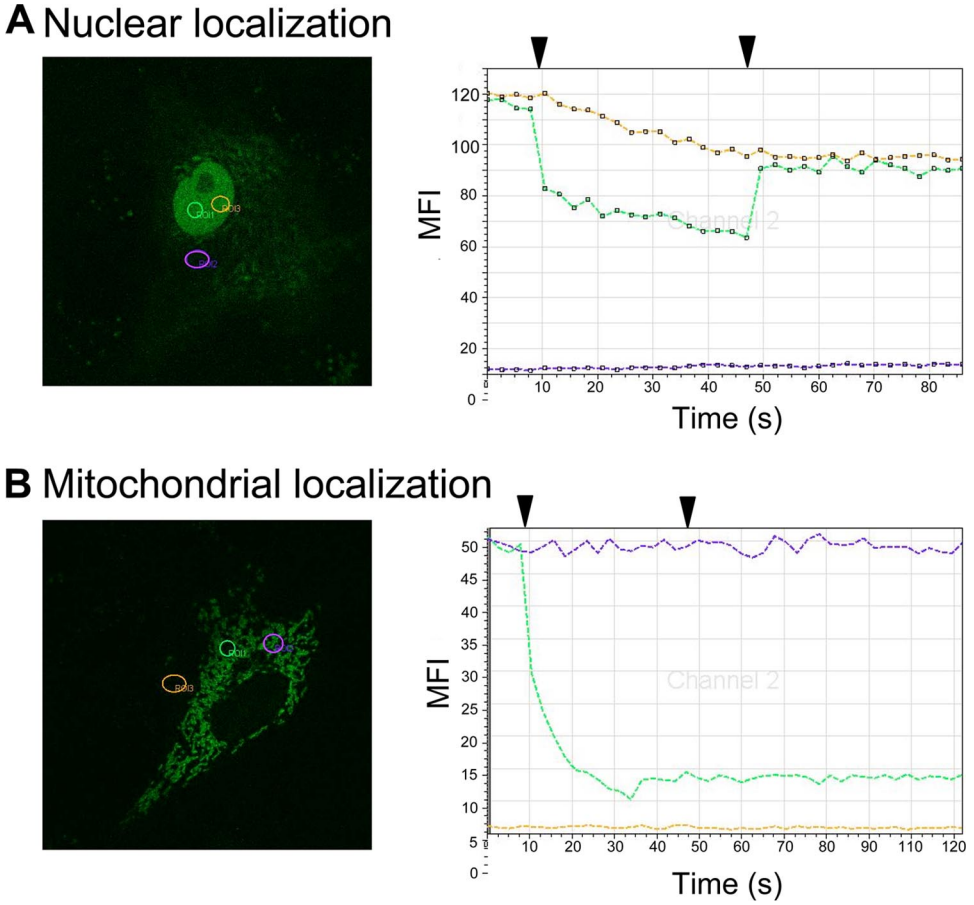

FIG. 2. FRAP analysis of nuclear and mitochondrial ORF 3b-EGFP. Vero cells were transfected with ORF 3b-EGFP, and cells expressing nuclear ORF 3b (A) or mitochondrial ORF 3b (B) were selected for analysis. (A) ROIs are shown that were photobleached (green), unbleached in the nucleus (orange), and an unbleached in the background (purple). (B) The photobleached ROI (green), an unbleached ROI including mitochondria (purple), and an unbleached ROI of background fluorescence (orange) are depicted. The time of bleaching is indicated on graphs by black arrowheads. FRAP was repeated two additional times, and similar results were obtained.

Spaciotemporal distribution of ORF 3b protein. To test whether the localization of ORF 3b protein changed as a function of time after expression, we performed time courses on individual cells. Within the first 4 h after expression became detectable, the ORF 3b protein accumulated solely in the nucleus. With time, however, the protein coincidentally disappeared from the nucleus and accumulated on mitochondria, thus leading to predominantly mitochondrial localization. It was possible to observe this redistribution on a single-cell level. Twenty-four hours after transfection, when the vast majority of transfected cells displayed mitochondrial localization of ORF 3b, a cell that expressed ORF 3b exclusively in the nucleus was selected for observation and imaged once per hour for 5 h (Fig. 1B). Initially, ORF 3b was undetectable in mitochondria, and the cell displayed strong nuclear fluorescence. Within 3 h, in this particular cell ORF 3b began to redistribute from the nucleus to mitochondria, and the fluorescence intensity in both organelles was equivalent. After 5 h, the redistribution was complete, with ORF 3b exclusively colocalized with mitochondria and none of the protein remaining in nuclei.

FRAP analysis of ORF 3b dynamics. The behavior of ORF 3b that we have described, whereby the protein initially accumulates in the nucleus prior to trafficking to mitochondria, has not been shown for any other viral protein. Furthermore, only a few examples of cellular proteins that translocate in a similar manner have been documented and include the transcription factors p53 and Nur77, both of which are thought to induce apoptosis after accumulating at mitochondria (27, 29, 30). Thus, this unique property of the ORF 3b protein warranted further characterization.

To determine whether the protein was stably associated with a subnuclear structure such as chromatin or was stably associated with mitochondria at later times, FRAP microscopy was utilized, which measures protein diffusion in live cells (3) (Fig. 2). Vero cells were transfected with the ORF 3b-EGFP plasmid, and single cells displaying nuclear or mitochondrial localization of ORF 3b-EGFP were analyzed. Photobleaching of a region of interest (ROI) within the nucleus resulted in decreased fluorescence within the ROI. The mean fluorescence intensity (MFI) of a separate nuclear ROI that was not subjected to photobleaching slowly decreased during the photobleaching period, suggesting rapid diffusion during the photobleaching process. Moreover, the nuclear MFI rapidly recovered within 2 s upon termination of photobleaching, further

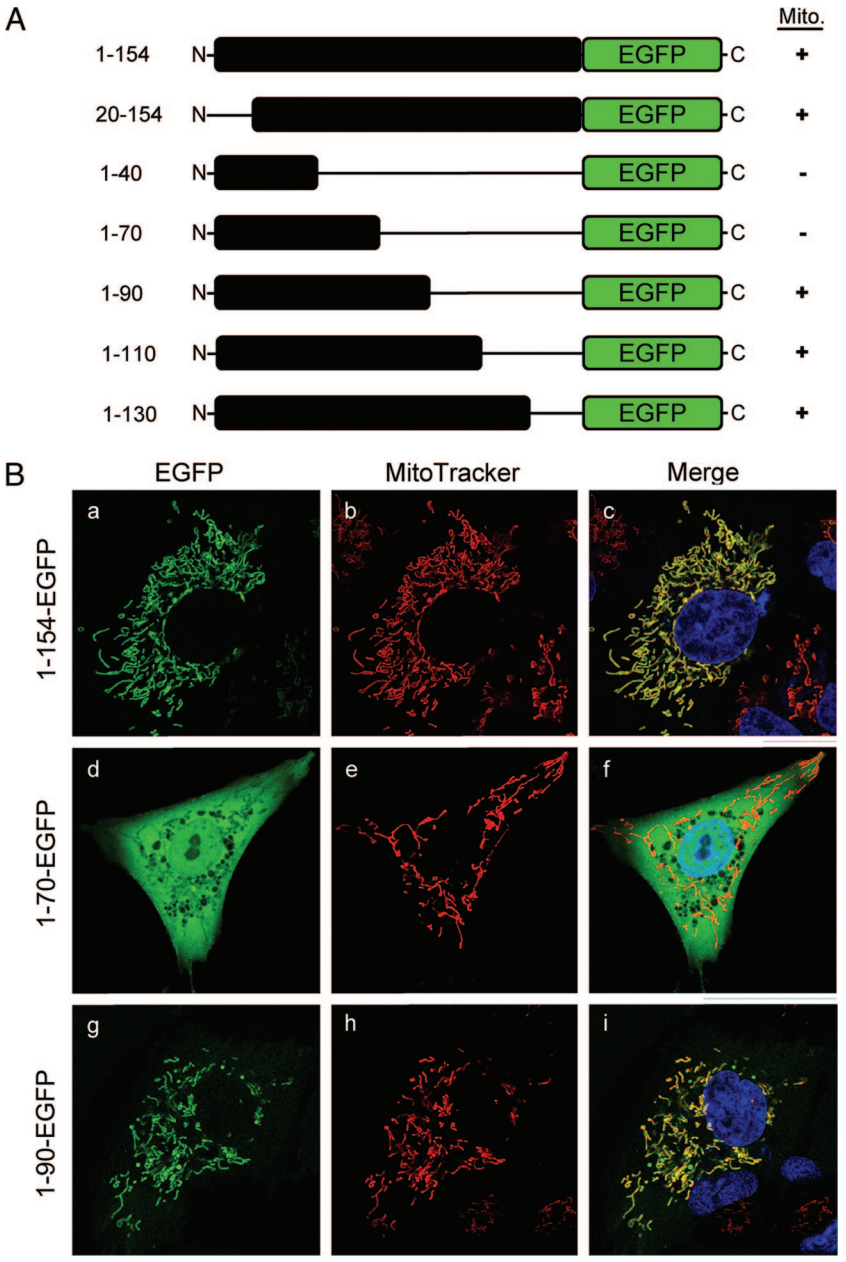

FIG. 3. Intracellular targeting of ORF 3b-EGFP truncations. (A) Schematic representation of C-terminal EGFP constructs used to determine the mitochondrial localization sequence. The ability of the constructs to localize to mitochondria (Mito) is indicated. (B) Vero cells were transfected with constructs encoding EGFP fusion proteins containing the full-length ORF 3b protein (1 to 154-EGFP) or truncations expressing residues 1 to 70 (1-70-EGFP) or 1 to 90 (1-90-EGFP), as indicated, and counterstained with MitoTracker (red) or Hoechst (blue) to identify mitochondria and nuclei, respectively, and observed by confocal microscopy at 24 hpt.

indicating rapid movement of the fluorescent protein within the nucleus (Fig. 2A). These results indicate that the ORF 3b protein is not stably associated with a static structure within the nucleus.

In contrast, we observed that mitochondrial ORF 3b-EGFP failed to recover upon termination of photobleaching (Fig. 2B). Consistent with stable mitochondrial association, a separate mitochondrial ROI within the same cell also showed no decrease in MFI during the time of the experiment. These results may indicate that the mitochondrial targeting sequence (MTS) of ORF 3b strongly interacts with the mitochondrial membrane but could also suggest that, upon translocation to mitochondria, ORF 3b binds a stably associated integral membrane protein.

Mitochondrial targeting via a predicted amphipathic α-helix. We next sought to identify the molecular determinants regulating subcellular localization of ORF 3b protein. To elucidate the mitochondrial localization domain, a series of truncations of ORF 3b was expressed as C-terminal fusions to EGFP (Fig. 3A). A web-based predictor of intracellular localization, PSORTII (http://psort.ims.u-tokyo.ac.jp/), identified a

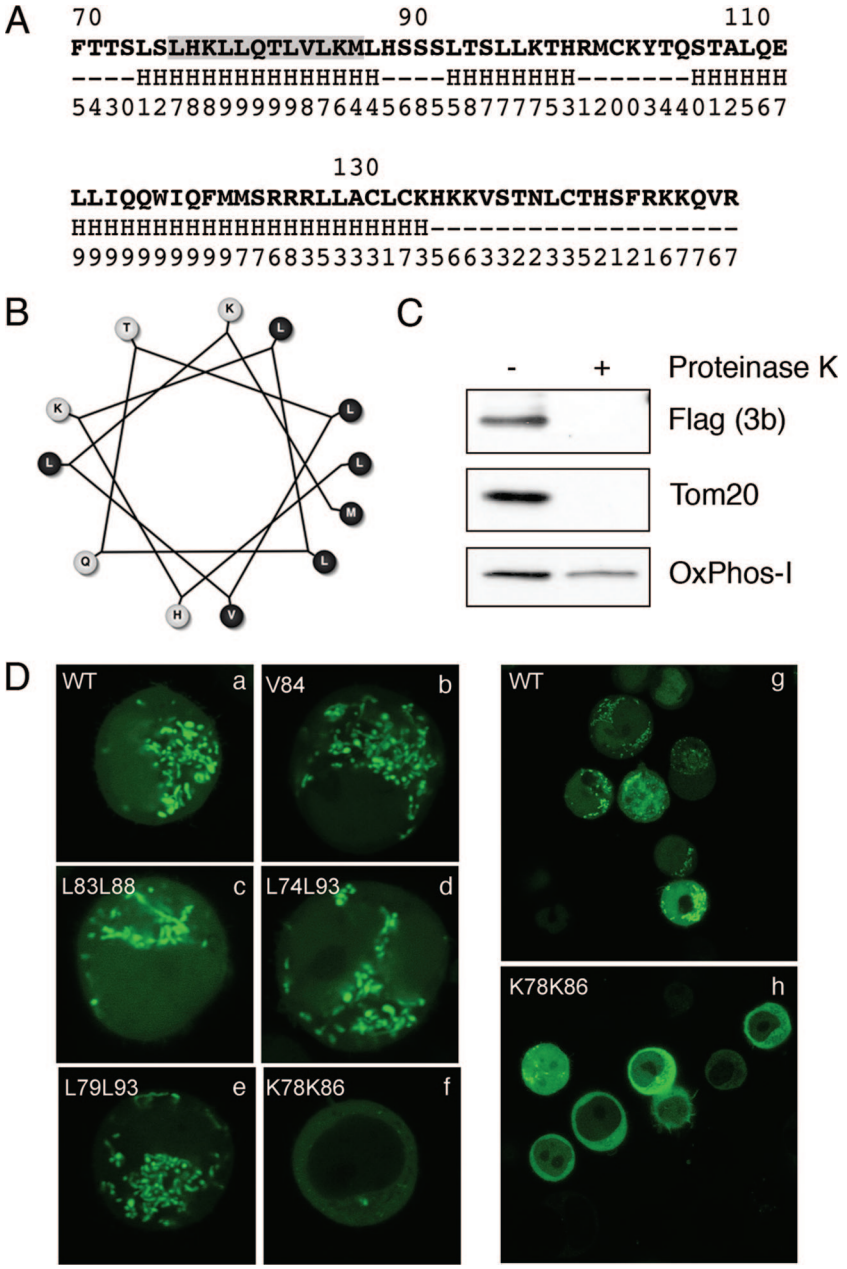

FIG. 4. Characterization of the mitochondrial targeting sequence of the ORF 3b protein. (A) The sequence of amino acids 70 to 154 of ORF 3b is shown with secondary structural predictions (H, helix) made by JPRED. Numbers indicate confidence of prediction (0, low; 9, high). (B) Helical wheel depiction of a predicted amphipathic helix formed by amino acids 74 to 85. (C) Protease protection assay. A mitochondrial fraction isolated from cells expressing pF-ORF 3b-EGFP was treated with proteinase K as described in Materials and Methods and subjected to immunoblotting to detect ORF 3b (anti-Flag), the outer mitochondrial transporter Tom20, or the internal mitochondrial protein OxPhos-I. (D) Mutational analysis of predicted helix. HEK293T cells were transfected with the indicated constructs and imaged by confocal microscopy at 24 hpt. Larger groups of cells expressing the unmutated ORF 3b protein (wild-type [WT]) and the K78K86 mutant are shown.

putative MTS in the first 20 amino acids of the protein. Surprisingly, deletion of these amino acids from ORF 3b failed to abolish mitochondrial localization. While the full-length protein displayed a mitochondrial pattern at 24 h (Fig. 3B, frames a to c), deletion of amino acids 71 to 154 caused a loss of mitochondrial localization, resulting in dispersal throughout the cytoplasm and a diffuse staining pattern (Fig. 3B, frames d to f). A similar expression pattern was observed for amino acids 1 to 40 (data not shown). Expression of amino acids 1 to 90 alone was sufficient to rescue mitochondrial targeting (Fig. 3B, frames g to i), indicating that important determinants for mitochondrial targeting reside within residues 71 to 90. Mitochondrial targeting was also achieved with all truncations that contained residues 20 to 70, including constructs expressing amino acids 1 to 110 and 1 to 130 (summarized in Fig. 3A).

Several other viral proteins have been shown to localize to mitochondria via an amphipathic α-helix often found in the C terminus of these proteins (1, 7, 15, 35). To assess whether

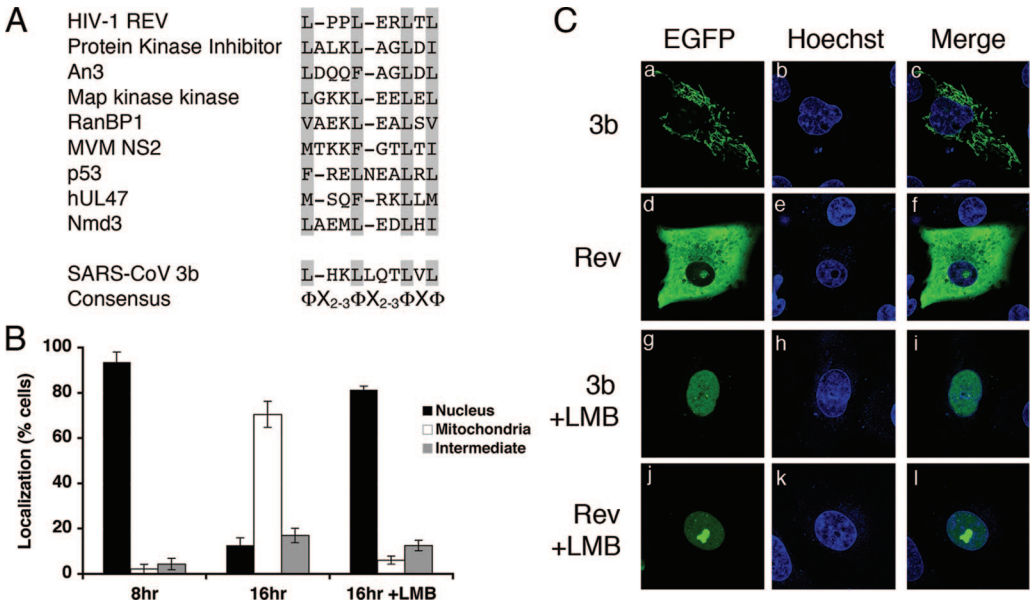

FIG. 5. Evidence for a functional nuclear export sequence in ORF 3b. (A) Protein sequence alignment of nuclear export motifs of proteins described to rely on CRM1-dependent nuclear export and ORF 3b (Φ is L, I, V, F, M; X is any amino acid). (B) Vero cells transfected with ORF 3b-EGFP were counted to determine the percentage displaying nuclear, mitochondrial, or both (intermediate) types of ORF 3b protein localization. Cells were scored at 8 hpt (n = 189 cells) and 16 hpt after incubation without (16 hr) (n = 186 cells) or with (16 hr+LMB) (n = 189 cells) 5 ng/ml LMB. Histograms show means ± standard deviations of three independent transfections. (C) Vero cells were transfected with ORF 3b-EGFP (3b) (a to c and g to i) or HIV Rev-EGFP (Rev) (d to f and j to l) and counterstained with Hoechst to demarcate nuclei. Transfected cells were incubated in the absence or presence of the specific inhibitor of CRM1-mediated export, LMB, as indicated.

ORF 3b possessed such an MTS, a secondary structural prediction was obtained for the C-terminal portion of the protein using the program JPRED (8). A helix was predicted between amino acids 70 to 90 (Fig. 4A). A helical wheel of this predicted helix (Fig. 4B) demonstrates the potential of residues 74 to 85 to form an amphipathic α-helix. To further refine the localization of ORF 3b, purified mitochondria were isolated from pF-ORF 3b-EGFP-expressing cells and subjected to proteinase K digestion and analysis by immunoblotting. In this assay, proteins on the outer mitochondrial membrane, such as Tom20, are digested by proteinase K while inner mitochondrial proteins, such as OxPhos-I, are protected from degradation. After treatment with proteinase K, it was no longer possible to detect ORF 3b by Western blotting. We therefore conclude that ORF 3b is bound to the outer membrane of the mitochondria (Fig. 4C).

To identify individual amino acids necessary for mitochondrial localization, we introduced mutations in the hydrophobic residues of the predicted amphipathic α-helix. Substitutions of alanine residues for Val 84, Leu 83 and 88, Leu 74 and 93, and Leu 79 and Leu 93 did not alter mitochondrial targeting (Fig. 4D). However, alanine substitutions for lysine residues 78 and 86 resulted in reduced mitochondrial targeting of the protein (Fig. 4D), suggesting a critical role for the positively charged residues in localization. The importance of positively charged amino acids in amphipathic α-helical mitochondrial targeting sequences has been previously documented in other viral proteins (15).

CRM1-mediated nuclear export. Sequence analysis suggested a putative consensus leucine-rich nuclear export sequence in the SARS-CoV ORF 3b (Fig. 5A), which likely binds CRM1 and mediates ORF 3b translocation and has been characterized in a number of proteins (12, 26, 37). To determine whether ORF 3b was actively transported out of the nucleus by CRM1, we tested the effect of the addition of LMB, a specific inhibitor of CRM1-mediated nuclear export (10, 13). In the absence of LMB, cells analyzed by confocal microscopy at 8 hpt displayed nuclear ORF 3b protein, whereas those examined at 16 hpt displayed mitochondrial ORF 3b. After LMB treatment, however, ORF 3b protein was retained in the nucleus, with very few cells showing mitochondrial localization (Fig. 5B). Consistent with our previous observations, we found that LMB-induced nuclear retention of ORF 3b correlated with a reduction in mitochondrial localization, confirming that nuclear accumulation of ORF 3b occurs prior to mitochondrial localization. These results also imply that the source of the mitochondrial pool is nuclear ORF 3b. As a control, human immunodeficiency virus type 1 (HIV-1) Rev, a protein known to rely on CRM1 for cytoplasmic localization, was found to be retained in the nucleolus by LMB (Fig. 5C).

Inhibition of type I IFN signaling. Recently, antagonistic roles for ORF 3b, ORF 6, and N protein in production of type I IFN were reported (25). However, the mechanism by which ORF 3b inhibits signaling for production of type I IFN is unknown. The MAVS protein responds to the detection of double-stranded RNA by RIG-I, which undergoes a conformational change upon binding of double-stranded RNA (39). MAVS leads to activation of Tank-binding kinase 1 and IκB kinaseε (IKKε) for phosphorylation and activation of IRF-3 and NF-κB. Mitochondrial localization of MAVS is known to be necessary for downstream signaling, suggesting that addi-

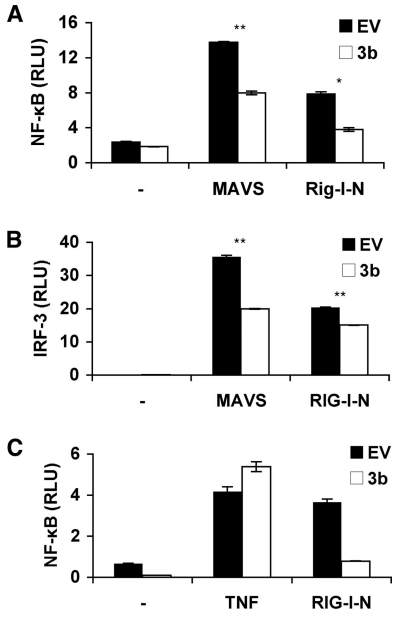

FIG. 6. SARS-CoV ORF 3b inhibits transcription factors for type I IFN signaling induced by overexpression of RIG-I-N or MAVS. Histograms of luciferase reporter activity from HEK293T cells cotransfected with Flag-myc ORF 3b (3b) or empty vector (EV) and an NF-κB reporter plasmid (A and C) or an IRF-3 reporter plasmid (B) and pRLTK and expression constructs for either pcDNA (−), MAVS, or RIG-I-N. Cells were lysed at 16 hpt, and both firefly and *Renilla* luciferase activities were measured. Luciferase activity was normalized to pRLTK signal and is depicted as RLU. (C) Cells were treated with 10 ng/ml human TNF-α (TNF) at 16 hpt for 6 h prior to analysis. Histograms representing RLU are shown ± standard deviations of three replicates. *, $P = 0.0003$; **, $P < 0.0001$ (unpaired Student's *t* test).

tional mitochondrial proteins may help activate Tank-binding kinase 1 and IκB kinase ε (14, 28).

We sought to determine whether ORF 3b protein inhibits type I IFN production by blocking MAVS activity at the mitochondria. To assess where ORF 3b has an inhibitory effect, HEK293T cells were transfected with a luciferase reporter plasmid driven by either the IRF-3-responsive element or the NF-κB promoter, Flag-myc-tagged ORF 3b, and expression constructs for MAVS or RIG-I-N, a constitutively active form of RIG-I. Upon overexpression of either RIG-I-N or MAVS, luciferase expression driven by IRF-3 and NF-κB was greatly increased. This effect was significantly reduced in the presence of ORF 3b (Fig. 6A and B). However, overexpression of ORF 3b did not inhibit activity of NF-κB induced by TNF-α, suggesting that the inhibitory effect of ORF 3b may be specific for the type I IFN pathway (Fig. 6C). These results confirm a direct inhibitory role of ORF 3b in the type I IFN antiviral response (25). Furthermore, since MAVS overexpression was not able to overcome inhibitory effect of ORF 3b, our data suggest that ORF 3b might inhibit MAVS at the mitochondria or that inhibition might occur downstream of MAVS in the signal transduction pathway.

DISCUSSION

The findings reported here are the first description, to our knowledge, of a virally encoded protein that initially accumulates in the nucleus and then entirely translocates to mitochondria. Many viral proteins that target mitochondria do so via amphipathic α-helices. Examples include HBx of hepatitis B virus, Vpr of HIV, p13 II of human T-cell leukemia virus type 1, and PB1-F2 of influenza A virus (1, 5, 9, 11, 15, 17, 20, 23). Intriguingly, nuclear localization has also been reported for each of these viral proteins, and nuclear export sequences have been described for both HBx and Vpr (11, 33). It remains to be determined if these proteins also undergo nucleo-mitochondrial shuttling. Nonetheless, our results attest to the necessity of evaluating the temporal distribution of viral proteins that appear to have complex spatial distributions in different cellular compartments.

The molecular mechanism regulating the timing of nucleo-mitochondrial translocation of ORF 3b protein remains to be determined. We have been unable to detect any evidence of posttranslational modifications of ORF 3b that could explain the localization behavior; ORF 3b isolated from a nuclear fraction has the same electrophoretic mobility as ORF 3b obtained from mitochondrial purification and does not appear to be phosphorylated (data not shown). We favor the hypothesis that ORF 3b undergoes a conformational change in the nucleus that exposes the MTS and nuclear export signal, which are encompassed in the same region of the protein, allowing for translocation out of the nucleus and to mitochondria. Our evidence would seem to suggest that a feature of the newly synthesized ORF 3b causes its continual uptake and inhibited egress from the nucleus since it appears to be mobile rather than tethered in the nucleus. Alternatively, it may be released in a time-dependent fashion from a fluid nuclear retention factor or acquire a mitochondrial location protein and thereby assume its specific localization via a partner protein(s). Although ORF 3b is sufficiently small to diffuse passively through the nuclear pore complex, the presence of active transport domains suggests that the SARS-CoV ORF 3b may act as a virally encoded chaperone and thus may bind and remove a host-encoded protein from the nucleus to modulate host responses during infection. The literature includes numerous examples of RNA viruses whose replication cycle occurs exclusively in the cytoplasm, like that of SARS-CoV, but that target the nucleus to facilitate replication or alter host cell function (18, 36).

Many virally encoded proteins target mitochondria to initiate or repress cellular suicide, or apoptosis (1, 2). We did not, however, observe features of apoptotic cell death upon expression of ORF 3b (E. C. Freundt and L. Yu, unpublished results). While very high expression of ORF 3b-EGFP caused a minor degree of cytotoxicity, we did not detect a loss of mitochondrial membrane potential as a result of mitochondrial accumulation of ORF 3b, nor did we observe mitochondrial release of cytochrome *c*, production of reactive oxygen species, or morphological features of apoptosis including nuclear condensation. Furthermore, ORF 3b overexpression did not confer resistance to mitochondrial pathways of apoptosis, including apoptosis induced with staurosporine (data not shown). However, these conclusions are limited by the fact that these experiments were performed by expressing ORF 3b on its own. Apoptotic or antiapoptotic activity of ORF 3b cannot therefore be entirely excluded as ORF 3b may have other mitochon-

drial functions that require the expression of additional SARS-CoV-encoded proteins, as would occur in a natural infection.

An important role for ORF 3b as an inhibitor of type I IFN expression has recently been described (25). In a previous study, overexpression of ORF 3b was shown to inhibit IRF-3 phosphorylation, reduce expression from an IFN-stimulated response element-driven reporter plasmid, and allow for replication of a type I IFN-sensitive virus, Newcastle disease virus. The mechanism by which ORF 3b blocks type I IFN production is unknown. MAVS is targeted by several virally encoded interferon antagonists (6, 28, 38). It is possible that ORF 3b targets this signaling pathway when it has reached the outer membrane of mitochondria. Work by Spiegel and colleagues demonstrated that during SARS-CoV infection, IRF-3 initially translocates to the nucleus at 8 h postinfection but is found redistributed in the cytoplasm at 16 h postinfection and fails to induce IFN-β expression (34). It is interesting that ORF 3b may influence this process since dynamics of ORF 3b nucleo-mitochondrial translocation occur within a similar time frame. Thus, our elucidation of the spatiotemporal distribution of the SARS-CoV ORF 3b protein may be important in understanding the mechanism by which SARS-CoV inhibits the IFN response.

ACKNOWLEDGMENTS

We thank Meggan Czapiga and Juraj Kabat, Biological Imaging Section, Research Technologies Branch, NIAID, for assistance with confocal microscopy.

This research was supported by the Intramural Research Program of the NIAID, National Institutes of Health. E.C.F. was supported by a National Institutes of Health-University of Oxford Biomedical Research Scholarship.

The findings and conclusions in this report are those of the authors and do not necessarily represent the views of the funding agency.

REFERENCES

1. **Boya, P., A. L. Pauleau, D. Poncet, R. A. Gonzalez-Polo, N. Zamzami, and G. Kroemer.** 2004. Viral proteins targeting mitochondria: controlling cell death. Biochim. Biophys. Acta **1659:**178–189.
2. **Boya, P., B. Roques, and G. Kroemer.** 2001. New EMBO members' review: viral and bacterial proteins regulating apoptosis at the mitochondrial level. EMBO J. **20:**4325–4331.
3. **Braga, J., J. M. Desterro, and M. Carmo-Fonseca.** 2004. Intracellular macromolecular mobility measured by fluorescence recovery after photobleaching with confocal laser scanning microscopes. Mol. Biol. Cell **15:**4749–4760.
4. **Chan, W. S., C. Wu, S. C. Chow, T. Cheung, K. F. To, W. K. Leung, P. K. Chan, K. C. Lee, H. K. Ng, D. M. Au, and A. W. Lo.** 2005. Coronaviral hypothetical and structural proteins were found in the intestinal surface enterocytes and pneumocytes of severe acute respiratory syndrome (SARS). Mod. Pathol. **18:**1432–1439.
5. **Chen, W., P. A. Calvo, D. Malide, J. Gibbs, U. Schubert, I. Bacik, S. Basta, R. O'Neill, J. Schickli, P. Palese, P. Henklein, J. R. Bennink, and J. W. Yewdell.** 2001. A novel influenza A virus mitochondrial protein that induces cell death. Nat. Med. **7:**1306–1312.
6. **Chen, Z., Y. Benureau, R. Rijnbrand, J. Yi, T. Wang, L. Warter, R. E. Lanford, S. A. Weinman, S. M. Lemon, A. Martin, and K. Li.** 2007. GB virus B disrupts RIG-I signaling by NS3/4A-mediated cleavage of the adaptor protein MAVS. J. Virol. **81:**964–976.
7. **Ciminale, V., L. Zotti, D. M. D'Agostino, T. Ferro, L. Casareto, G. Franchini, P. Bernardi, and L. Chieco-Bianchi.** 1999. Mitochondrial targeting of the p13II protein coded by the x-II ORF of human T-cell leukemia/lymphotropic virus type I (HTLV-I). Oncogene **18:**4505–4514.
8. **Cuff, J. A., M. E. Clamp, A. S. Siddiqui, M. Finlay, and G. J. Barton.** 1998. JPred: a consensus secondary structure prediction server. Bioinformatics **14:**892–893.
9. **D'Agostino, D. M., L. Ranzato, G. Arrigoni, I. Cavallari, F. Belleudi, M. R. Torrisi, M. Silic-Benussi, T. Ferro, V. Petronilli, O. Marin, L. Chieco-Bianchi, P. Bernardi, and V. Ciminale.** 2002. Mitochondrial alterations induced by the p13II protein of human T-cell leukemia virus type 1. Critical role of arginine residues. J. Biol. Chem. **277:**34424–34433.
10. **Fischer, U., J. Huber, W. C. Boelens, I. W. Mattaj, and R. Luhrmann.** 1995. The HIV-1 Rev. activation domain is a nuclear export signal that accesses an export pathway used by specific cellular RNAs. Cell **82:**475–483.
11. **Forgues, M., A. J. Marrogi, E. A. Spillare, C. G. Wu, Q. Yang, M. Yoshida, and X. W. Wang.** 2001. Interaction of the hepatitis B virus X protein with the Crm1-dependent nuclear export pathway. J. Biol. Chem. **276:**22797–22803.
12. **Fornerod, M., and M. Ohno.** 2002. Exportin-mediated nuclear export of proteins and ribonucleoproteins. Results Probl. Cell Differ. **35:**67–91.
13. **Fornerod, M., M. Ohno, M. Yoshida, and I. W. Mattaj.** 1997. CRM1 is an export receptor for leucine-rich nuclear export signals. Cell **90:**1051–1060.
14. **Freundt, E. C., and M. J. Lenardo.** 2005. Interfering with interferons: hepatitis C virus counters innate immunity. Proc. Natl. Acad. Sci. USA **102:**17539–17540.
15. **Gibbs, J. S., D. Malide, F. Hornung, J. R. Bennink, and J. W. Yewdell.** 2003. The influenza A virus PB1-F2 protein targets the inner mitochondrial membrane via a predicted basic amphipathic helix that disrupts mitochondrial function. J. Virol. **77:**7214–7224.
16. **Guo, J. P., M. Petric, W. Campbell, and P. L. McGeer.** 2004. SARS corona virus peptides recognized by antibodies in the sera of convalescent cases. Virology **324:**251–256.
17. **Henkler, F., J. Hoare, N. Waseem, R. D. Goldin, M. J. McGarvey, R. Koshy, and I. A. King.** 2001. Intracellular localization of the hepatitis B virus HBx protein. J. Gen. Virol. **82:**871–882.
18. **Hiscox, J. A.** 2003. The interaction of animal cytoplasmic RNA viruses with the nucleus to facilitate replication. Virus Res. **95:**13–22.
19. **Holmes, K. V., and L. Enjuanes.** 2003. Virology. The SARS coronavirus: a postgenomic era. Science **300:**1377–1378.
20. **Hou, X., S. Foley, M. Cueto, and M. A. Robinson.** 2000. The human T-cell leukemia virus type I (HTLV-I) X region encoded protein p13(II) interacts with cellular proteins. Virology **277:**127–135.
21. **Huang, C., C. J. Peters, and S. Makino.** 2007. Severe acute respiratory syndrome coronavirus accessory protein 6 is a virion-associated protein and is released from 6 protein-expressing cells. J. Virol. **81:**5423–5426.
22. **Ito, N., E. C. Mossel, K. Narayanan, V. L. Popov, C. Huang, T. Inoue, C. J. Peters, and S. Makino.** 2005. Severe acute respiratory syndrome coronavirus 3a protein is a viral structural protein. J. Virol. **79:**3182–3186.
23. **Jacotot, E., L. Ravagnan, M. Loeffler, K. F. Ferri, H. L. Vieira, N. Zamzami, P. Costantini, S. Druillennec, J. Hoebeke, J. P. Briand, T. Irinopoulou, E. Daugas, S. A. Susin, D. Cointe, Z. H. Xie, J. C. Reed, B. P. Roques, and G. Kroemer.** 2000. The HIV-1 viral protein R induces apoptosis via a direct effect on the mitochondrial permeability transition pore. J. Exp. Med. **191:**33–46.
24. **Khan, S., B. C. Fielding, T. H. Tan, C. F. Chou, S. Shen, S. G. Lim, W. Hong, and Y. J. Tan.** 2006. Over-expression of severe acute respiratory syndrome coronavirus 3b protein induces both apoptosis and necrosis in Vero E6 cells. Virus Res. **122:**20–27.
25. **Kopecky-Bromberg, S. A., L. Martinez-Sobrido, M. Frieman, R. A. Baric, and P. Palese.** 2007. Severe acute respiratory syndrome coronavirus open reading frame (ORF) 3b, ORF 6, and nucleocapsid proteins function as interferon antagonists. J. Virol. **81:**548–557.
26. **Kutay, U., and S. Guttinger.** 2005. Leucine-rich nuclear-export signals: born to be weak. Trends Cell Biol. **15:**121–124.
27. **Li, H., S. K. Kolluri, J. Gu, M. I. Dawson, X. Cao, P. D. Hobbs, B. Lin, G. Chen, J. Lu, F. Lin, Z. Xie, J. A. Fontana, J. C. Reed, and X. Zhang.** 2000. Cytochrome c release and apoptosis induced by mitochondrial targeting of nuclear orphan receptor TR3. Science **289:**1159–1164.
28. **Li, X. D., L. Sun, R. B. Seth, G. Pineda, and Z. J. Chen.** 2005. Hepatitis C virus protease NS3/4A cleaves mitochondrial antiviral signaling protein off the mitochondria to evade innate immunity. Proc. Natl. Acad. Sci. USA **102:**17717–17722.
29. **Marchenko, N. D., A. Zaika, and U. M. Moll.** 2000. Death signal-induced localization of p53 protein to mitochondria. A potential role in apoptotic signaling. J. Biol. Chem. **275:**16202–16212.
30. **Moll, U. M., N. Marchenko, and X. K. Zhang.** 2006. p53 and Nur77/TR3—transcription factors that directly target mitochondria for cell death induction. Oncogene **25:**4725–4743.
31. **Navas-Martin, S., and S. R. Weiss.** 2003. SARS: lessons learned from other coronaviruses. Viral Immunol. **16:**461–474.
32. **Rota, P. A., M. S. Oberste, S. S. Monroe, W. A. Nix, R. Campagnoli, J. P. Icenogle, S. Penaranda, B. Bankamp, K. Maher, M. H. Chen, S. Tong, A. Tamin, L. Lowe, M. Frace, J. L. DeRisi, Q. Chen, D. Wang, D. D. Erdman, T. C. Peret, C. Burns, T. G. Ksiazek, P. E. Rollin, A. Sanchez, S. Liffick, B. Holloway, J. Limor, K. McCaustland, M. Olsen-Rasmussen, R. Fouchier, S. Gunther, A. D. Osterhaus, C. Drosten, M. A. Pallansch, L. J. Anderson, and W. J. Bellini.** 2003. Characterization of a novel coronavirus associated with severe acute respiratory syndrome. Science **300:**1394–1399.
33. **Sherman, M. P., C. M. de Noronha, M. I. Heusch, S. Greene, and W. C. Greene.** 2001. Nucleocytoplasmic shuttling by human immunodeficiency virus type 1 Vpr. J. Virol. **75:**1522–1532.
34. **Spiegel, M., A. Pichlmair, L. Martinez-Sobrido, J. Cros, A. Garcia-Sastre, O. Haller, and F. Weber.** 2005. Inhibition of beta interferon induction by severe

acute respiratory syndrome coronavirus suggests a two-step model for activation of interferon regulatory factor 3. J. Virol. **79:**2079–2086.

35. **Suzuki, R., S. Sakamoto, T. Tsutsumi, A. Rikimaru, K. Tanaka, T. Shimoike, K. Moriishi, T. Iwasaki, K. Mizumoto, Y. Matsuura, T. Miyamura, and T. Suzuki.** 2005. Molecular determinants for subcellular localization of hepatitis C virus core protein. J. Virol. **79:**1271–1281.
36. **Weidman, M. K., R. Sharma, S. Raychaudhuri, P. Kundu, W. Tsai, and A. Dasgupta.** 2003. The interaction of cytoplasmic RNA viruses with the nucleus. Virus Res. **95:**75–85.
37. **Williams, P., J. Verhagen, and G. Elliott.** 2008. Characterization of a CRM1-dependent nuclear export signal in the C terminus of herpes simplex virus type 1 tegument protein UL47. J. Virol. **82:**10946–10952.
38. **Yang, Y., Y. Liang, L. Qu, Z. Chen, M. Yi, K. Li, and S. M. Lemon.** 2007. Disruption of innate immunity due to mitochondrial targeting of a picornaviral protease precursor. Proc. Natl. Acad. Sci. USA **104:**7253–7258.
39. **Yoneyama, M., M. Kikuchi, T. Natsukawa, N. Shinobu, T. Imaizumi, M. Miyagishi, K. Taira, S. Akira, and T. Fujita.** 2004. The RNA helicase RIG-I has an essential function in double-stranded RNA-induced innate antiviral responses. Nat. Immunol. **5:**730–737.
40. **Yount, B., R. S. Roberts, A. C. Sims, D. Deming, M. B. Frieman, J. Sparks, M. R. Denison, N. Davis, and R. S. Baric.** 2005. Severe acute respiratory syndrome coronavirus group-specific open reading frames encode nonessential functions for replication in cell cultures and mice. J. Virol. **79:**14909–14922.
41. **Yuan, X., Y. Shan, Z. Yao, J. Li, Z. Zhao, J. Chen, and Y. Cong.** 2006. Mitochondrial location of severe acute respiratory syndrome coronavirus 3b protein. Mol. Cells **21:**186–191.
42. **Yuan, X., Y. Shan, Z. Zhao, J. Chen, and Y. Cong.** 2005. G0/G1 arrest and apoptosis induced by SARS-CoV 3b protein in transfected cells. Virol. J. **2:**66.
43. **Yuan, X., Z. Yao, Y. Shan, B. Chen, Z. Yang, J. Wu, Z. Zhao, J. Chen, and Y. Cong.** 2005. Nucleolar localization of non-structural protein 3b, a protein specifically encoded by the severe acute respiratory syndrome coronavirus. Virus Res. **114:**70–79.
44. **Zheng, L., O. Schickling, M. E. Peter, and M. J. Lenardo.** 2001. The death effector domain-associated factor plays distinct regulatory roles in the nucleus and cytoplasm. J. Biol. Chem. **276:**31945–31952.